Structural Eng./Earthquake Eng., JSCE, Vol. 15, No. 1, 29s—39s, 1998 January
(J. Struct. Mech. Earthquake Eng., JSCE, No. 584/ I —42)

MODELING WAVE PROPAGATION BY USING NORMALIZED INPUT-OUTPUT MINIMIZATION (NIOM) METHOD FOR MULTIPLE LINEAR SYSTEMS

Hamid R. HADDADI[1] and Hideji KAWAKAMI[2]

[1]Ph.D. student of Earthquake Engineering, Dept. of Civil & Environmental Eng., Saitama University (255 Shimo-Okubo, Urawa, Saitama 338, Japan)
[2]Member of JSCE, Dr. of Eng., Professor, Dept. of Civil & Environmental Eng., Saitama University (255 Shimo-Okubo, Urawa, Saitama 338, Japan)

Consideration of simple models of wave propagation helps to understand the physical characteristics of soil layers. In this paper, a new method for modeling wave propagation in multiple linear systems is developed, its application is discussed and the results are compared with those of conventional correlation, impulse response and geophysical methods. The new method reveals the arrival times of incident and reflected waves as well as their relative amplitudes. The effects of weighting coefficients on Fourier amplitude spectrum of the results are also discussed for some models and actual strong ground motion records.

Key Words : *wave propagation, spectral analysis, vertical array, wave amplification*

1. INTRODUCTION

Closely spaced seismograph arrays are widely employed to record the strong ground motion on the surface or at lower elevations of ground. Those records are used to study the spatial as well as temporal variation of ground motion[1)-6)] and provide the essential information for seismic design of largely extended foundation structures, deeply embedded or buried facilities and lifeline systems.

Actual earthquake ground motions reflect the characteristics of the source mechanism, wave propagation path and amplification effect of the soil layers. However, those effects cannot be recognized directly from the records due to complexity of actual ground motions. Therefore, some methods are used either to simplify the ground motion source (such as geophysical methods) or to make simplified models of wave propagation (such as impulse response and correlation functions).

Propagation of wave through ground layers is studied by using geophysical methods in which an impulsive seismic source can be generated by explosion or impact. The arrival times of the generated waves by such a simple seismic source would be detected easily at different points on the ground surface or at different depths. These methods are widely employed for evaluating the dynamic properties of soil. However, the parameters estimated by such methods are rather different from those during a strong earthquake motion, which is much more complicated.

When ground motion at one observation point repeats itself exactly at another point and noise is not involved in the motion, an impulse may be assumed to be a simple model of ground motion at one location and the impulse response would be obtained at the other by means of the soil system transfer function. Actual earthquake motions are much complicated and this ideal model usually fails to reveal the properties of the soil system.

The other model that can relate motions at two locations is the cross-correlation. For the case of completely coherent motion, it is equal to the autocorrelation of the motion at one observation point but shifted by a time lag or advance. Actual earthquake motions may contain superposed waves that are reflected and refracted from various interfaces. Therefore, the cross-correlation of the

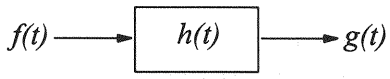

Fig.1 A time-invariant linear soil system

motions at two observation points would not be simply the shifted results of the autocorrelation. Further, the shape of cross-correlation function is greatly influenced by the wave propagation properties and by the shape of the autocorrelation function which causes some limitations in practice.

This paper presents a new method for modeling wave propagation in multiple linear systems by considering the statistical correlation of the earthquake ground motions at different observation points. The paper describes the capability of the presented method in comparison with the other existing methods by using some models as well as actual strong ground motion records.

2. METHODOLOGY

(1) One linear soil system

A time-invariant linear soil system (**Fig.1**) subjected to the input earthquake motion, $f(t)$, at the ground surface and the output $g(t)$ at depth is defined by means of the convolution integral[7]

$$g(t) = \int_{-\infty}^{\infty} h(u)f(t-u)du \qquad (1)$$

where $h(u)$ is the weight function.

The input and output of the system in the frequency domain can be related by means of the transfer function $H(\omega)$. For the case that the input and output of the system are digitized earthquake ground motions, the output at each frequency is specified by[7]

$$G(\omega_i) = H(\omega_i)F(\omega_i) \qquad (2)$$
$$(i = 0, ..., N-1 \text{ and } \omega_i = i\frac{2\pi}{N\Delta t})$$

where Δt is the sampling rate in the time domain and N is the number of samples. $F(\omega_i)$ and $G(\omega_i)$ are the Fourier transforms of the digitized earthquake motion at the ground surface and at depth .

Transfer functions depend only on physical properties of soil systems. Therefore the same transfer function that defines the relation of the actual ground motion input, $F(\omega_i)$, and output, $G(\omega_i)$, should satisfy the relation of the input model, $X(\omega_i)$, and the output model, $Y(\omega_i)$, as follows.

$$Y(\omega_i) = H(\omega_i)X(\omega_i) \qquad (3)$$

Consider the discrete inverse Fourier transform of $X(\omega_i)$

$$x(m\Delta t) = \frac{1}{N\Delta t}\sum_{i=0}^{N-1} X(\omega_i)e^{j\frac{2\pi im}{N}} \qquad (4)$$

and assume that the amplitude of the input is desired to be constant at an arbitrary time such as t=0. Therefore, Eq.(4) gives the following constraint.

$$\frac{1}{N\Delta t}\sum_{i=0}^{N-1} X(\omega_i) = 1 \qquad (5)$$

Eq.(5) implies that the value of the input at the ground surface for $m = 0$ (which corresponds to $t = 0$ in the time domain) is defined to be normalized to unity.

Using the method of Lagrange multipliers, squared Fourier amplitude spectra[8] of the ground motions at the surface and at depth are minimized when subjected to the constraint of Eq.(5). Therefore the Lagrange multipliers method gives

$$L = \sum_{i=0}^{N-1}\left\{|X(\omega_i)|^2 + |Y(\omega_i)|^2\right\} - \lambda\left\{\frac{1}{N\Delta t}\sum_{i=0}^{N-1} X(\omega_i) - 1\right\} \qquad (6)$$

where λ is the Lagrange multiplier. Summation of square values in Eq.(6) corresponds to the power of the input and output. A simplified model of input and output would be obtained by minimizing Eq.(6). When the constraint is considered, the simplified input is modeled such that its amplitude at t=0 is unity and the simplified input and output amplitudes approach zero at the other times unless correlation exists between the corresponding ordinates. If there is not any constraint in Eq.(6), the minimization procedure gives zero input and zero output at all times and it does not give any useful result. Substituting Eq.(3) into Eq.(6) gives

$$L = \sum_{i=0}^{N-1}\left\{1 + |H(\omega_i)|^2\right\}X(\omega_i)X^*(\omega_i) - \lambda\left\{\frac{1}{N\Delta t}\sum_{i=0}^{N-1} X(\omega_i) - 1\right\} \qquad (7)$$

in which * denotes the complex conjugate .

One may find $X(\omega_i)$ with minimum L by requiring $\frac{\partial L}{\partial X(\omega_i)} = 0$ and $\frac{\partial L}{\partial X^*(\omega_i)} = 0$. This gives λ as:

$$\lambda = \frac{2(N\Delta t)^2}{\sum_{i=0}^{N-1} \frac{1}{1+|H(\omega_i)|^2}} \tag{8}$$

Consequently, the simplified ground motions of the system would be determined by the following equations:

$$X(\omega_i) = N\Delta t \frac{\frac{1}{1+|H(\omega_i)|^2}}{\sum_{n=0}^{N-1} \frac{1}{1+|H(\omega_n)|^2}} \tag{9}$$

$$Y(\omega_i) = N\Delta t \frac{\frac{H(\omega_i)}{1+|H(\omega_i)|^2}}{\sum_{n=0}^{N-1} \frac{1}{1+|H(\omega_n)|^2}} \tag{10}$$

Eq.(10) is the response of the linear system to the simplified input model of Eq.(9). The same transfer function that satisfies the relationship of the actual ground motion input and output is used to derive Eq.(10). As a result, the complicated strong motions of the input and output are modeled to a simple pair that reveals the relation of the actual strong motions and yields useful information about the propagation of waves through the system.

The procedure leading to the simplified input and output models is shown schematically in **Fig.2**. As **Fig.2** shows, the actual ground motion input, $F(\omega_i)$, and output, $G(\omega_i)$, are used to compute the transfer function, $H(\omega_i)$. Minimizing the square values of Fourier amplitude spectra at the surface and at depth when the constraint is in existence would result in the simplified input model of $X(\omega_i)$ and the simplified output model of $Y(\omega_i)$, which illustrates the statistical correlation between the two motions. This process is named the Normalized Input-Output Minimization (NIOM) method. The inverse Fourier transform of Eq.(9) gives the input model at the ground surface in the time domain and the corresponding model at depth would be obtained by the inverse Fourier transform of Eq.(10).

(2) Frequency content and smoothing of the results

High frequency components of the ground motion are known to be more susceptible to scattering and attenuation and those components do not correlate to the corresponding ones at the other observation points. Also, the noise accompanying earthquake ground motion can affect the results and cause fluctuations. Therefore, it is useful to have a control on the contribution of the frequency components in the process. Consider $dx(t)/dt$ and

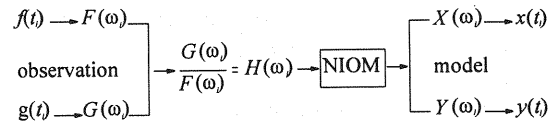

Fig.2 The schematic procedure of the NIOM method

$dy(t)/dt$ are also taken into account and the square values of their Fourier amplitude spectra are minimized and properly weighted. Therefore, the Lagrange multipliers method gives the following equation:

$$\begin{aligned} L = \sum_{i=0}^{N-1} \{ & c_0 |X(\omega_i)|^2 + k_0 \omega_i^2 |X(\omega_i)|^2 \\ & + c_1 |Y(\omega_i)|^2 + k_1 \omega_i^2 |Y(\omega_i)|^2 \} \\ & - \lambda \left\{ \frac{1}{N\Delta t} \sum_{i=0}^{N-1} X(\omega_i) - 1 \right\} \end{aligned} \tag{11}$$

in which the constraint of Eq.(5) is used and c_0, c_1, k_0 and k_1 are weighting constants.

One may again find $X(\omega_i)$ and $Y(\omega_i)$ with minimum L by requiring $\frac{\partial L}{\partial X(\omega_i)} = \frac{\partial L}{\partial X^*(\omega_i)} = 0$ as follows:

$$X(\omega_i) = N\Delta t \frac{\frac{1}{(1+\frac{k_0}{c_0}\omega_i^{\ 2})(c_0+c_1|H(\omega_i)|^2)}}{\sum_{n=0}^{N-1} \frac{1}{(1+\frac{k_0}{c_0}\omega_n^{\ 2})(c_0+c_1|H(\omega_n)|^2)}} \tag{12}$$

$$Y(\omega_i) = N\Delta t \frac{\frac{H(\omega_i)}{(1+\frac{k_0}{c_0}\omega_i^2)(c_0+c_1|H(\omega_i)|^2)}}{\sum_{n=0}^{N-1} \frac{1}{(1+\frac{k_0}{c_0}\omega_n^2)(c_0+c_1|H(\omega_n)|^2)}} \tag{13}$$

Eqs.(12) and (13) assume that the relationship between the weighting constants is

$$\frac{k_0}{c_0} = \frac{k_1}{c_1} \tag{14}$$

which implies that the same weighting relationship between the squared Fourier amplitude spectra of the input and its time derivative is considered for the output.

One may keep the value of one of the coefficients constant in Eq.(14). In this case, c_0 is fixed to unity in the process. The coefficient k_1 is computed in terms of the other weighting constants. Therefore, it is enough to specify k_0 and c_1 in the computations. The contribution of high frequencies may be decreased by increasing k_0 in Eqs.(12) and (13) (This is shown later in **Figs.5** and **9**). Therefore high frequency components of the input and output, which may be scattered or attenuated, play a smaller role in the process. The coefficient c_1 weights the output in comparison to

the input. When c_1 increases, the contribution of the output in the process increases.

If c_1 and k_0 approach zero in Eqs.(12) and (13), the simplified input in the frequency domain is:

$$X(\omega_i) = \Delta t \quad \text{for } i = 0, ..., N-1 \tag{15}$$

This implies that the simplified input in the time domain would approach the impulse function and therefore that the simplified output would approach the impulse response. The effect of the weighting constants is discussed later when the application of the method is explained.

(3) Generalization to multiple linear systems

M linear systems are subjected to the input $x(t)$, and the outputs are named $y_1(t)$ to $y_M(t)$. Therefore, the following value is minimized under the same constraint of Eq.(5).

$$\sum_{i=0}^{N-1}\Big[c_0|X(\omega_i)|^2 + k_0\omega_i^2|X(\omega_i)|^2 + \sum_{l=1}^{M}\left\{c_l|Y_l(\omega_i)|^2 + k_l\omega_i^2|Y_l(\omega_i)|^2\right\}\Big] \tag{16}$$

In Eq.(16), c_0 to c_M are the weighting constants of the input and outputs squared Fourier amplitude spectra, and k_0 to k_M are those of their time derivatives. The multiple linear system is considered as a number of single linear systems such that the input is common in all. For each single system, the relation between the weighting constants of the input squared Fourier amplitude spectra and its time derivative is considered to be equal to that of the output. Therefore, the weighting coefficients are related as:

$$\frac{k_0}{c_0} = \frac{k_1}{c_1} = ... = \frac{k_M}{c_M} \tag{17}$$

Considering Eq.(17) and the transfer function of the single linear system l as

$$H_l(\omega_i) = \frac{Y_l(\omega_i)}{X(\omega_i)} \tag{18}$$

then, Lagrange multipliers method gives:

$$L = \sum_{i=0}^{N-1}\left\{\left(1 + \sum_{l=1}^{M}\frac{c_l}{c_0}|H_l(\omega_i)|^2\right)\cdot\left(c_0 + k_0\omega_i^2\right)X(\omega_i)X^*(\omega_i)\right\} - \lambda\left\{\frac{1}{N\Delta t}\sum_{i=0}^{N-1}X(\omega_i) - 1\right\} \tag{19}$$

One may find $X(\omega_i)$ with minimum L by requiring $\frac{\partial L}{\partial X(\omega_i)} = 0$ and $\frac{\partial L}{\partial X^*(\omega_i)} = 0$. Thus, λ can be obtained as follows:

$$\lambda = \frac{2(N\Delta t)^2}{\sum_{i=0}^{N-1}\frac{1}{(1+\frac{k_0}{c_0}\omega_i^2)(c_0+\sum_{l=1}^{M}c_l|H_l(\omega_i)|^2)}} \tag{20}$$

Some algebraic manipulation leads to the following equations for the simplified input and outputs.

$$X(\omega_i) = N\Delta t\frac{\frac{1}{(1+\frac{k_0}{c_0}\omega_i^2)(c_0+\sum_{m=1}^{M}c_m|H_m(\omega_i)|^2)}}{\sum_{n=0}^{N-1}\frac{1}{(1+\frac{k_0}{c_0}\omega_n^2)(c_0+\sum_{m=1}^{M}c_m|H_m(\omega_n)|^2)}} \tag{21}$$

$$Y_l(\omega_i) = N\Delta t\frac{\frac{H_l(\omega_i)}{(1+\frac{k_0}{c_0}\omega_i^2)(c_0+\sum_{m=1}^{M}c_m|H_m(\omega_i)|^2)}}{\sum_{n=0}^{N-1}\frac{1}{(1+\frac{k_0}{c_0}\omega_n^2)(c_0+\sum_{m=1}^{M}c_m|H_m(\omega_n)|^2)}} \tag{22}$$

$Y_l(\omega_i)$ is obtained by substituting Eq.(21) into Eq.(18).

In case of multiple linear systems, if c_0=1 and k_1 to k_M are substituted in terms of the other weighting constants then it is enough to specify only k_0 and c_1 to c_M.

Generalization of the method to multiple linear systems gives more realistic results. In this case, all the ground motions at different observation points are processed simultaneously, whereas in a single input-output system the results are based on the ground motion records at only two observation points.

(4) Dimensionless Fourier amplitude spectrum

The Fourier amplitude spectrum of the input and outputs, obtained from Eqs.(21) and (22), can be used in dimensionless form. This form is needed for comparing one set of Fourier spectra to another set in which the sampling rate is different. Eqs.(23) and (24) show the dimensionless forms of the input and output models respectively. It should be noted that $x(t_i)$ and $y(t_i)$ are dimensionless while $f(t_i)$ and $g(t_i)$ may have dimensions (see **Fig.2**).

$$\frac{X(\omega_i)}{\Delta t} = N\frac{\frac{1}{\left\{1+\frac{k_0/\Delta t^2}{c_0}(\omega_i\Delta t)^2\right\}(1+\sum_{m=1}^{M}\frac{c_m}{c_0}|H_m(\omega_i)|^2)}}{\sum_{n=0}^{N-1}\frac{1}{\left\{1+\frac{k_0/\Delta t^2}{c_0}(\omega_n\Delta t)^2\right\}(1+\sum_{m=1}^{M}\frac{c_m}{c_0}|H_m(\omega_n)|^2)}} \tag{23}$$

$$\frac{Y_I(\omega_i)}{\Delta t} = N \frac{\dfrac{H_I(\omega_i)}{\left\{1+\frac{k_0/\Delta t^2}{c_0}(\omega_i \Delta t)^2\right\}\left(1+\sum_{m=1}^{M}\frac{c_m}{c_0}|H_m(\omega_i)|^2\right)}}{\sum_{n=0}^{N-1}\dfrac{1}{\left\{1+\frac{k_0/\Delta t^2}{c_0}(\omega_n \Delta t)^2\right\}\left(1+\sum_{m=1}^{M}\frac{c_m}{c_0}|H_m(\omega_n)|^2\right)}} \tag{24}$$

3. APPLICATION OF THE METHOD TO SIMPLE MODELS

To clarify the effectiveness of the NIOM method, the results of the method are compared here with the results obtained when using conventional autocorrelation, cross-correlation, and impulse response methods by using simple models. The models are made by means of a time history and applying successive shifting and adding. The time history $f(t)$ is considered as the input and the following combinations are assumed to be the outputs of the linear systems.

$$g_1(t) = 4f(t) + n(t) \tag{25a}$$
$$g_2(t) = 4f(t) + 3f(t-\tau) + n(t) \tag{25b}$$
$$g_3(t) = 4f(t) + 3f(t-\tau) + 2f(t-2\tau) + n(t) \tag{25c}$$
$$g_4(t) = 4f(t) + 3f(t-\tau) + 2f(t-2\tau) + f(t-3\tau) + n(t) \tag{25d}$$

The simplified input and output of the system are obtained by transforming the results of Eqs.(12) and (13) into the time domain. The results by the NIOM method are obtained for two cases. In the first case, the input and output are not accompanied by white noise ($n(t) = 0$). **Fig.3** corresponds to this case and the results of the NIOM method are compared with the results obtained by the conventional autocorrelation and cross-correlation methods and with those of conventional impulse response function. In the second case, the input and output are accompanied by white noise $n(t)$. The results of this case are shown in **Fig.4** and compared with the other two methods. The weighting constants of c_0=1, c_1=0.001, k_0=0.001 and the sampling rate $\Delta t = 0.01$ sec are used for the models mentioned in this section.

The first column in **Figs.3** and **4** shows the input of $f(t)$ and the outputs of Eqs.(25a) to (25d) for $\tau = 0.1$ sec. The second column shows the autocorrelation of $f(t)$ at the top and cross-correlation of $f(t)$ and $g_1(t)$, $g_2(t)$, $g_3(t)$ and $g_4(t)$ below that. The third column shows the unit impulse function at the top and the unit impulse responses below that. The fourth column shows the simplified input of the NIOM method at the top and the simplified outputs below that. As **Figs.3** and **4** show, the results of the NIOM method clearly present the relationship of the input and the different outputs as one expects from Eqs.(25a) to (25d), whereas the results of correlation and impulse response methods do not. Comparison between the third column in **Figs.3** and **4** indicates that the impulse response method is much affected by noise.

While cross-correlation method is usually more useful for the case that ensemble strong ground motion records are available[9], **Figs.3** and **4** show that even by considering one input and one output, the NIOM method is potential to reveal the relation of the input and output.

As mentioned in section 2(2), the contribution of frequency bands in the process can be determined by specifying the weighting constant k_0. The effect of k_0 on the frequency band of the input model (the top figure at the fourth column of **Fig.3**) obtained by applying the NIOM method to the input and the output of Eq.(25a) is illustrated in **Fig.5**. In this figure, the dimensionless Fourier amplitude spectrum is shown for various values of $k=k_0/(c_0\Delta t^2)$ and it indicates that the contributions of high frequencies are decreased when k is increased. The coefficient c_1/c_0 does not effect on the results in this case. As Eqs.(23) and (24) show, c_1/c_0 is also effective when the transfer function is not constant. However, **Fig.5** can be considered as a representative simplified Fourier amplitude spectrum of the results by the NIOM method. The effect of the weighting constant k is similar to that of high cut filtering.

4. ANALYSIS OF THE ETCHUJIMA STRONG MOTION RECORDS

The acceleration time histories recorded at the Etchujima vertical array[10] during the earthquakes M6.0 of February 27, 1983, M6.0 of August 8, 1983, and M6.7 of December 17, 1987, are used in this analysis. **Table 1** shows the geological profile, density of the layers, and elastic wave velocities measured by downhole shooting. The observation points of the array are located at elevations GL-1.0 m, GL-40.0 m, and GL-100.0 m. **Fig.6** shows the acceleration ground motion (NS component) of the earthquake M6.0 of February 27, 1983, recorded at different elevations of the vertical array.

The results of the analysis by using the generalized NIOM method for multiple linear systems are shown in **Fig.7**. Based on the geophysical and geological information, the arrival

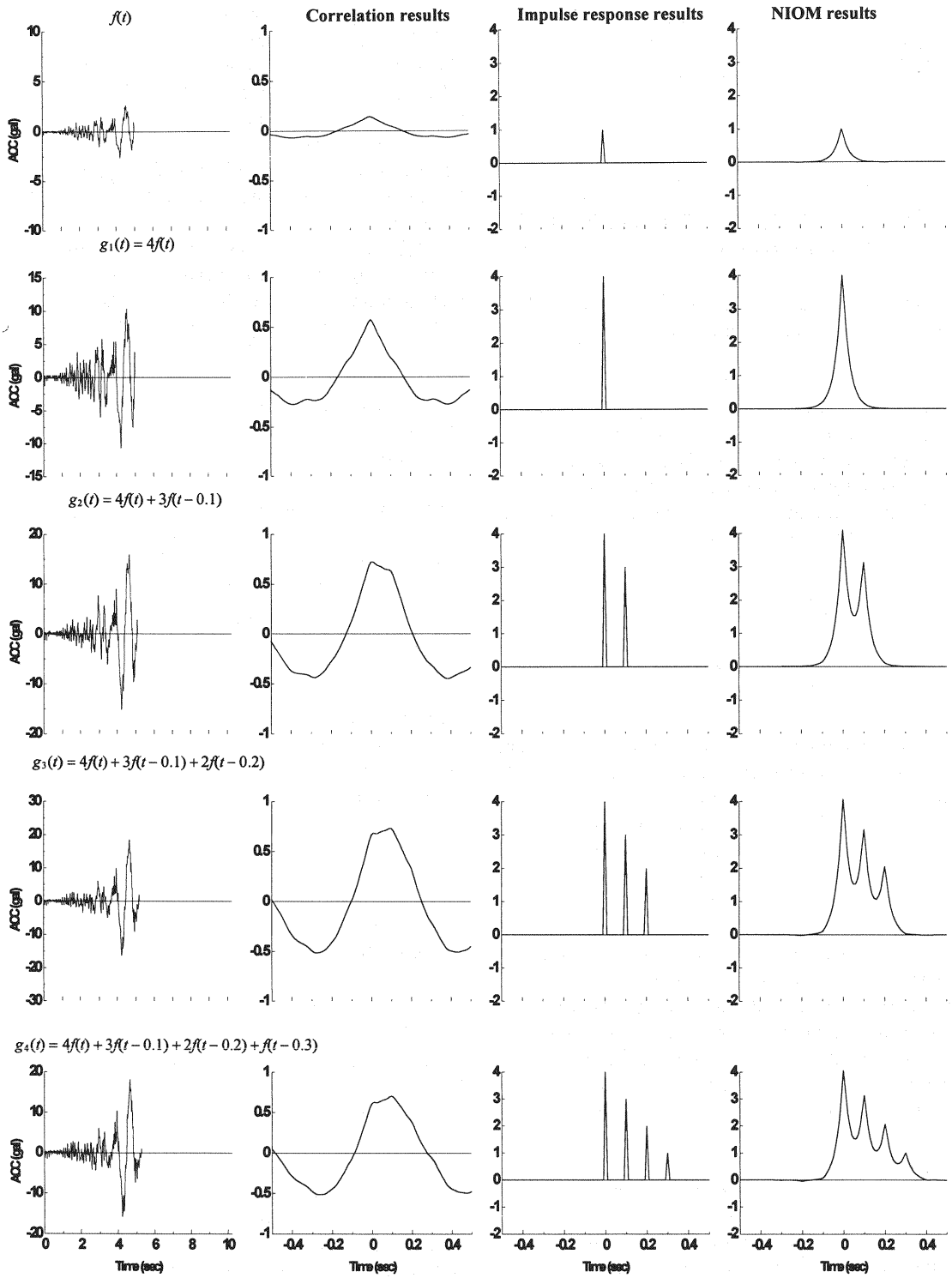

Fig.3 Application of the NIOM method to simple models and comparison with the results obtained by the correlation and impulse response methods. The first column shows the strong motion time history considered as the input $f(t)$ and some combinations of that as the outputs $g_1(t)$ to $g_4(t)$. The second column shows the autocorrelation of $f(t)$ at the top and cross-correlation of $f(t)$ and $g_1(t)$ to $g_4(t)$ below that respectively. The third column shows the unit impulse function at the top and the impulse responses for different cases below that. The fourth column shows the simplified input by the NIOM at the top and the responses to the simplified input below that.

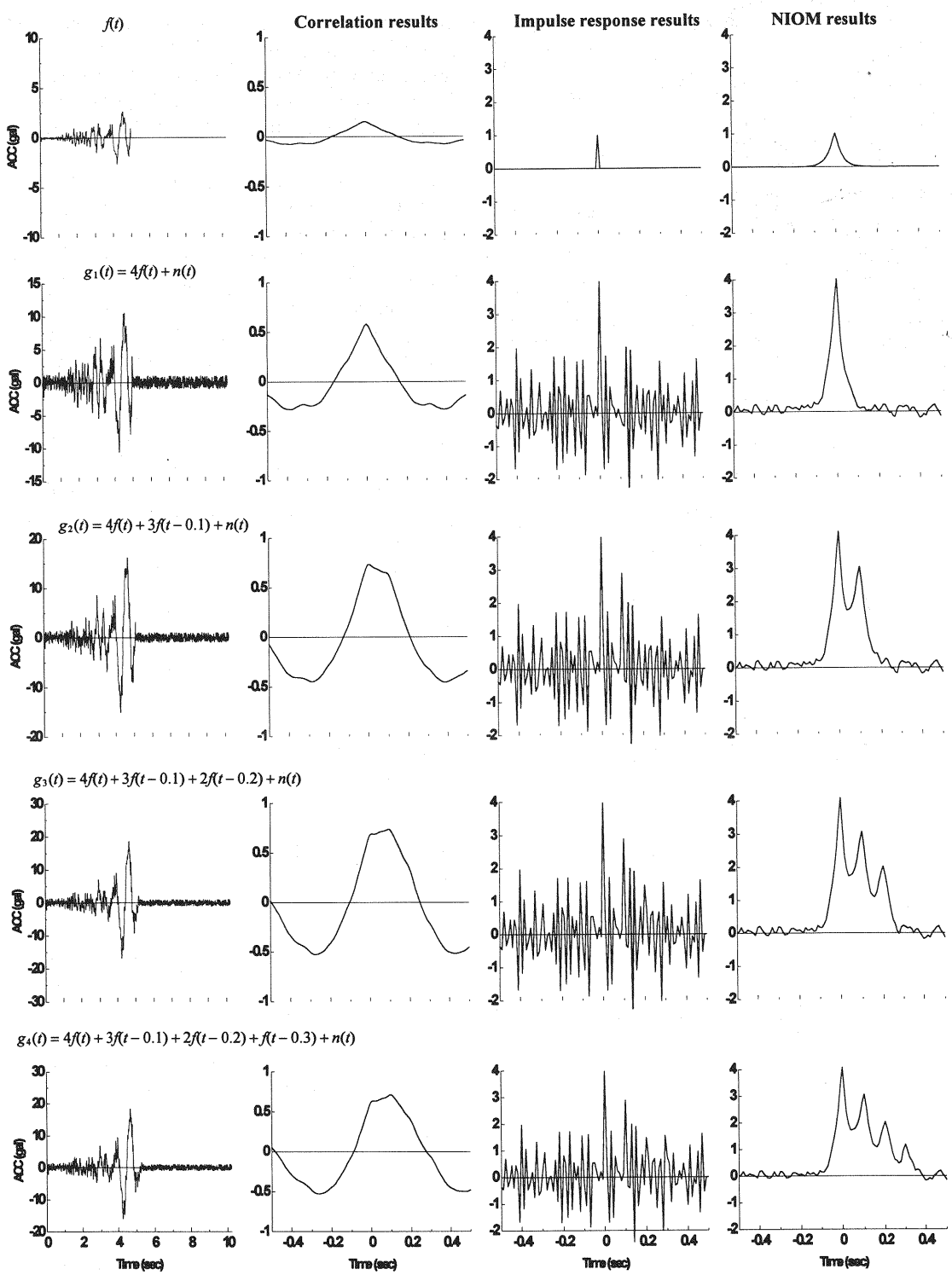

Fig.4 Application of the NIOM method to simple models and comparison with the results obtained by the correlation and impulse response methods. The first column shows the strong motion time history considered as the input $f(t)$ and some combinations of that plus the white noise $n(t)$ as the outputs $g_1(t)$ to $g_4(t)$. The second column shows the autocorrelation of $f(t)$ at the top and cross-correlation of $f(t)$ and $g_1(t)$ to $g_4(t)$ below that respectively. The third column shows the unit impulse function at the top and the impulse responses for different cases below that. The fourth column shows the simplified input by the NIOM at the top and the responses to the simplified input below that.

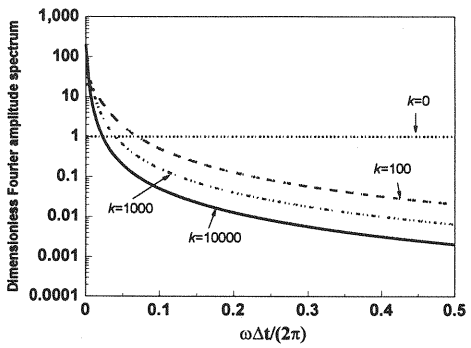

Fig.5 Dimensionless Fourier amplitude spectrum of the simplified input model obtained by the NIOM method for the input of $f(t)$ and the output of Eq.(25a).

Table 1 Geological and geophysical information of the Etchujima site.

Depth (m)	Type	Density (g/cm³)	P-wave velocity (km/sec)	S-wave velocity (km/sec)	Location of seismometer
0~4	sandy silt	1.7	0.62	0.11	GL-1.0 m
4~10			0.94		
10~16	alluvial clay	1.6		0.13	
16~26			1.33		
26~34	sandy silt	1.7		0.23	
34~38			0.93		
38~53	sandy gravel	2		0.44	GL-40.0 m
53~70					
70~75	fine sand	1.85	1.75	0.3	
75~83				0.46	
83~100	mudstone	1.9			GL-100.0 m

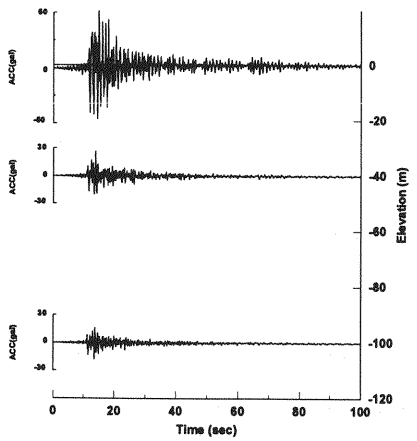

Fig.6 The NS component strong motion time history of the earthquake M6.0 of February 27,1983 recorded at the Etchujima site.

times of S-wave and P-wave are computed and shown in the figure. The figure shows the simplified input and the simplified responses at different observation points. The simplified input is obtained at elevation GL-1.0 m and the responses are computed and shown at GL-40.0 m and GL-100.0 m. The weighting constants of $c_0=c_1=c_2=1$, $k_0=0.0001$ and the sampling rate $\Delta t=0.03$ sec are used in this analysis.

The simplified outputs computed by using the horizontal strong motion records (**Fig.7**, EW and NS components) show two clear peaks corresponding to the incident S-wave and the reflected S-wave from the ground surface at GL-40.0 m and GL-100.0 m. The results are compared with the arrival times obtained by the downhole well shooting and show good agreement. The mentioned peaks are stable and are observed at both the horizontal component responses for all the three analyzed events. Some other peaks are also observed at GL-40.0 m and GL-100.0 m of the horizontal components. Those peaks are recognized to be stable for different components and earthquakes and are believed to reflect the geological conditions.

The simplified outputs computed by applying the generalized form of the NIOM method to the vertical strong motion records of the three earthquakes (**Fig.7**, UD component) also show clear peaks which are in agreement with the elastic P-wave arrival times obtained by downhole well shooting. The remarkable achievement of analyzing the vertical strong motion records is that the vertical simplified outputs at GL-40.0 m and GL-100.0 m of all the three earthquakes do not show any peak corresponding to the S-wave propagation. This is also confirmed by analyzing the S-portions of the vertical component strong motions. The results of analyzing only the S-portions of the vertical component strong motion records for the three events are shown in **Fig.8**. This analysis shows that the S-portions of the vertical strong motions also propagate in P-wave velocity.

The effect of $k_0/(c_0\Delta t^2)$ on the NIOM results is confirmed for the actual ground motion records. **Fig.9** shows the dimensionless Fourier amplitude spectra of the input model for various values of $k=k_0/(c_0\Delta t^2)$ obtained by the NIOM method, for the earthquake of Feb. 27, 1983, recorded at the Etchujima site. The actual ground motion records also show the same trend of dimensionless Fourier amplitude spectra as obtained for the simple model

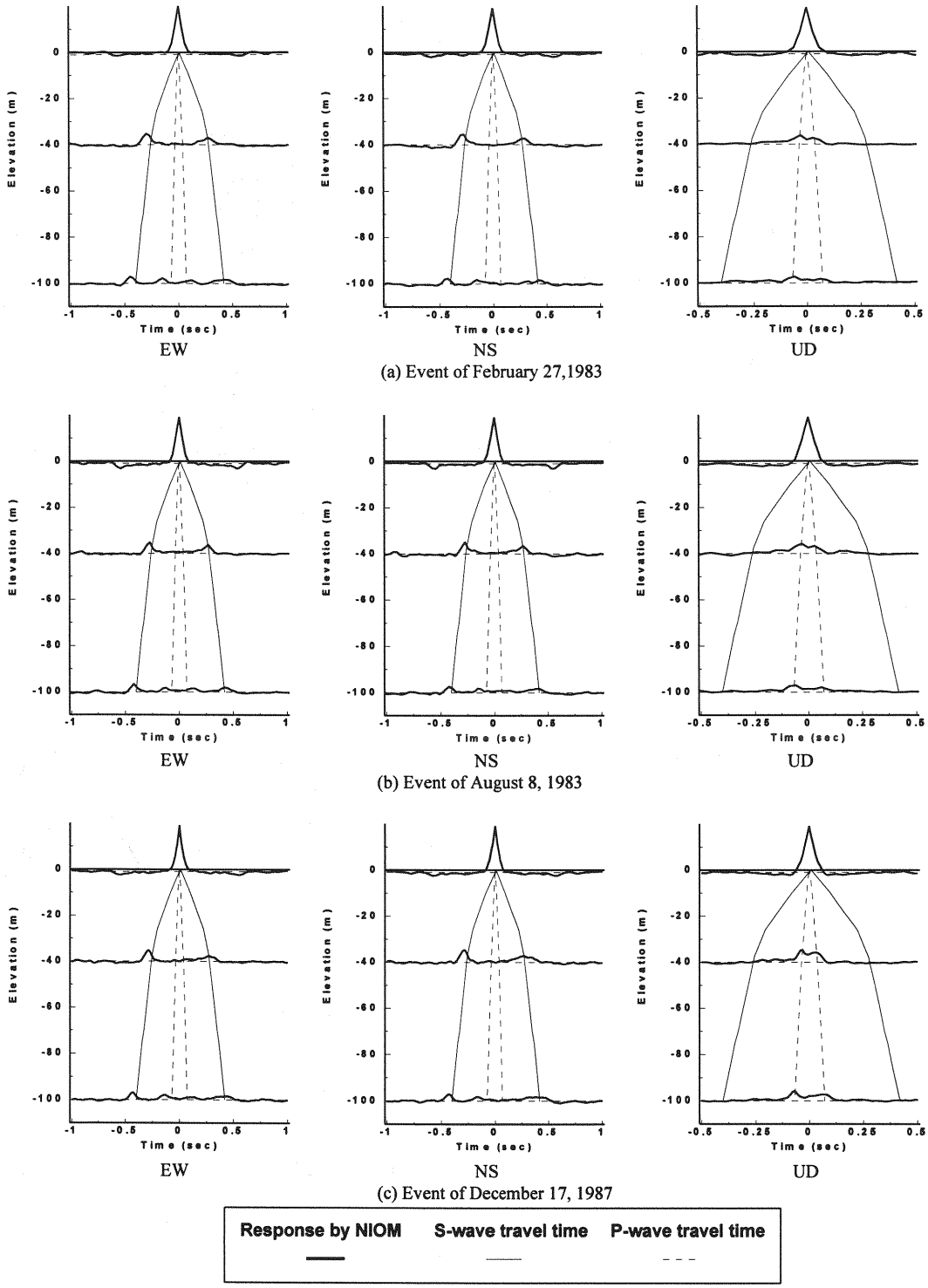

Fig.7 The results obtained by the NIOM method in comparison with the P-wave and S-wave elastic velocities measured by downhole well shooting at the Etchujima site. Three components (EW, NS and UD) of strong ground motion are considered in the analysis of each event.

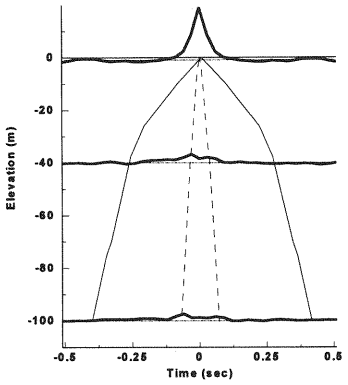

a) Event of Feb. 27, 1983

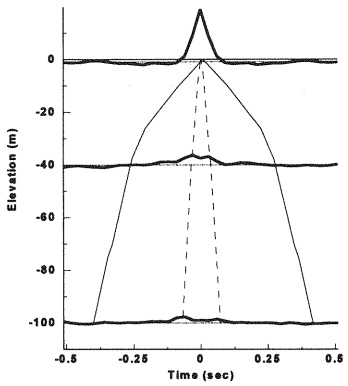

b) Event of August 8, 1983

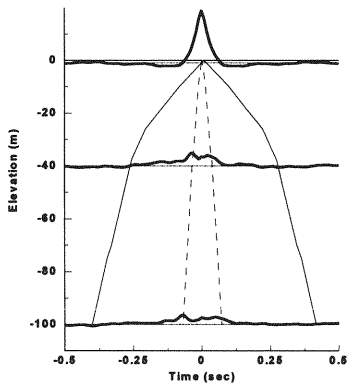

c) Event of December 17, 1987

Fig.8 Analysis of the S-portions of the vertical component strong motion time histories by the NIOM method and comparison with the results of downhole well shooting. (Legend is the same as **Fig.7**)

of **Fig.5**. The effect of the constant k is similar to that of high cut filtering.

The method also shows the effect of soil amplification in **Fig.7**. Significant differences are

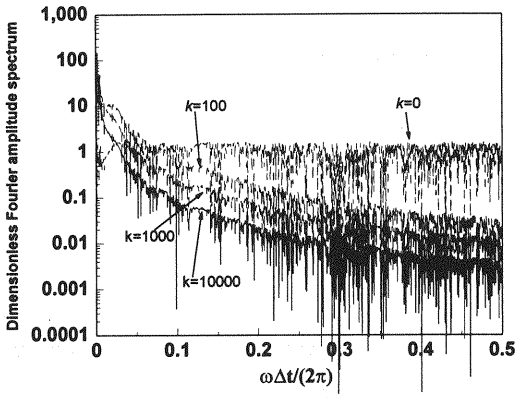

Fig.9 Dimensionless Fourier amplitude spectra of the NIOM input model for the earthquake of 27 Feb., 1983 at the Etchujima site.

observed between the amplitude of the peaks at deeper layers and the relating peaks at shallower layers, and implies that the waves are amplified mostly in the layers from elevation GL-40.0 m to the ground surface.

The incident and reflected peaks revealed by the NIOM method also show a reasonable relationship between the amplitude of the incident wave and the reflected wave. The reflected wave amplitude is smaller than the incident amplitude which is in accordance with the multiple reflection theory.

5. CONCLUSIONS AND DISCUSSIONS

1) The Normalized Input-Output Minimization (NIOM) method is capable of revealing a simplified relationship between the input and outputs of linear systems. The results obtained by applying the method to simple models, including one time history as the input and some different combinations of that as the outputs, reveal a distinct correlation between the input and the outputs, and the method is shown to be more effective than the conventional cross-correlation and impulse response methods.

The generalized NIOM method has potential for simultaneous processing of strong ground motions recorded at different observation points of vertical and/or horizontal seismic arrays.

2) Application of the method to the records of the Etchujima vertical array yields clear arrival times for the incident and reflected S-waves and P-waves. The results agree with the downhole well shooting measurements at the site.

The analysis of horizontal components of the three earthquakes at the Etchujima site shows clear peaks that agree with the S-wave arrival times.

3) The vertical component responses by the NIOM method show clear peaks for the incident and reflected waves that agree with the P-wave arrival times obtained by downhole well shooting. The remarkable result is that the responses of the vertical strong motions do not show any peak due to propagation of S-wave. This is also confirmed by analyzing the separated S-portion of the vertical strong motions.

4) There is also a reasonable relationship between the amplitudes of the incident and reflected waves in the shallow layers. The amplitude of the reflected wave from the ground surface is smaller than that of the incident wave, which is consistent with the multiple reflection theory.

The method also shows the effect of shallow layers on the wave amplification at the Etchujima site. The layers from GL-40.0 m up to the ground surface have significantly larger effect on amplification of the wave than do the deeper layers at the site.

5) The effects of weighting coefficients on Fourier amplitude spectrum of the results are also discussed for some models as well as actual strong ground motion records. The NIOM method clearly shows the simplified correlation of input and outputs of linear systems and is useful for studying wave propagation in shallow layers.

6) The NIOM method has also potential for processing the horizontal and/or vertical components of ground motion records at the same or different observation points which is useful for studying the propagation of surface waves. This application is also considered by the authors and the results will be published in a separate paper.

7) When considering "estimation of the system", the problem is usually up to obtaining $H(\omega)$ in Eq.(2). The transfer function, $H(\omega)$, is sometimes estimated by the method of least squares. This estimated transfer function may be used in the NIOM method instead of that obtained by Eq.(2). In the proposed NIOM method, square values are minimized as in the least variance estimation method. The difference between these two methods is that the latter method minimizes summation of square values of errors whereas in the NIOM method that of signals is minimized.

ACKNOWLEDGMENTS: The authors express their thanks to the Association for Earthquake Disaster Prevention of Japan for publishing the strong motion array record database. They also acknowledge Shimizu Corporation for providing the strong motion records at the Etchujima vertical array.

REFERENCES

1) Bolt, B. A., Tsai, T. B., Yeh, K. and Hsu, M. K. : Earthquake strong motion recorded by large near-source array of digital seismographs, *Earthquake Engrg. and Struct. Dyn.*, 10, 561- 573, 1982.
2) Loh, C. H., Penzien, J. and Tsai, Y. B.: Engineering analysis of SMART-1 array accelerometers, *Earthquake Engrg. and Struct. Dyn.*, 10, 575-591, 1982.
3) Nakamura, H. and Yamazaki, F.: Spatial correlation of earthquake ground motion based on dense array records, *J. of Structural Mechanics and Earthquake Engineering*, JSCE, No. 519, I-32, 185-197, 1995.
4) Vanmarcke, E. H. and Harichandran, R. S.: Models of the spatial variation of earthquake ground motion for seismic analysis of structures. *Proc. 8th World Conf. on Earthquake Engrg., San Francisco, Calif.*, 1984.
5) Kausel, E. and Pais, A.: Stochastic deconvolution of earthquake motions, *J. Engrg. Mech.*, ASCE, 113(2), 266-277, 1987.
6) Hoshiya, M. and Ishii, K.: Evaluation of kinematic interaction of soil foundation systems by a stochastic model, *Soil Dyn. and Earthquake Engrg.*, 2(3), 128-134, 1983.
7) Bendat, J. S. and Piersol, A. G.: *Random data: analysis and measurement procedures*, John Wiley & Sons, 1971.
8) Clough, R. W. and Penzien, J.: *Dynamics of structures*, McGraw-Hill, Inc, 1993.
9) Izumi, M., Kurita, S., Iizuka, S., Sato, T. and Aiba, T.: On the coherency and the characteristics of transfer functions between seismic waves with instrument array, *J. of Structural and Construction Engineering*, Trans. AIJ. No. 395, 28-39, 1989 (in Japanese).
10) Association for Earthquake Disaster Prevention of Japan: Strong motion array record database, data manual, Volume A01, July 1992.

(Received October 9, 1996)